Journal Pre-proof

NiO-nanoflowers decorating a plastic electrode for the non-enzymatic amperometric detection of H2O2 in milk: Old issue, new challenge

M. Carbone, E. Aneggi, F. Figueredo, S. Susmel

PII: S0956-7135(21)00687-3

DOI: https://doi.org/10.1016/j.foodcont.2021.108549

Reference: JFCO 108549

To appear in: *Food Control*

Received Date: 17 June 2021

Revised Date: 3 September 2021

Accepted Date: 6 September 2021

Please cite this article as: Carbone M., Aneggi E., Figueredo F. & Susmel S., NiO-nanoflowers decorating a plastic electrode for the non-enzymatic amperometric detection of H2O2 in milk: Old issue, new challenge, *Food Control* (2021), doi: https://doi.org/10.1016/j.foodcont.2021.108549.

Conceptualization	Sabina Susmel,
Investigation	Sabina Susmel, Eleonora Aneggi, Marilena Carbone
Formal analysis Investigation, Data Curation	Sabina Susmel, Eleonora Aneggi, Marilena Carbone, Federico Figueredo
Resources	Sabina Susmel, Marilena Carbone
Writing - Original Draft	Sabina Susmel, Federico Figueredo, Marilena Carbone
Writing - Review & Editing	Sabina Susmel, Federico Figueredo, Eelonora Aneggi,
Visualization	Sabina Susmel, Federico Figueredo, Marilena Carbone, Eleonora Aneggi
Supervision, Project administration, Funding acquisition	Sabina Susmel

NiO-*nanoflowers* decorating a plastic electrode for the non-enzymatic amperometric detection of H_2O_2 in milk: old issue, new challenge

M. Carbone [a], E. Aneggi [b], F. Figueredo [c,d] and S. Susmel [c],*

[a] Department of Chemical Science and Technologies, University of Rome Tor Vergata, Via della Ricerca Scientifica 1, 00133 Rome, IT

[b] Polytechnic Department, University of Udine, Via del Cotonificio 108, 33100 Udine, IT

[c] Department of Agricultural, Food, Environmental and Animal Sciences (Di4A), BioAnalytical Chemistry Lab (UBAC), Chemistry Section, University of Udine, Via del Cotonificio 108, 33100 Udine, IT

[d] Present address: Laboratory of Biosensors and Bioanalysis (LABB), Biological Chemistry Department and IQUIBICEN-CONICET, Science School, University of Buenos Aires, Buenos Aires, Argentina.

* Sabina.Susmel@uniud.it; tel. + 39 (0)432558823; fax. +39(0)432558803

Keywords

Milk, PVC composite electrode, Nickel Oxide, H_2O_2 amperometric sensing, disinfection.

Abstract

In food supply chain, there are regulatory limitations on the use of chemicals for cleaning processing lines since the healthiness of the commodities must be guaranteed if accidentally traces of these detergents and sanitizers pass to them. Hydrogen peroxide, is a commonly used sanitizer in the cleaning of the food processing lines having both bactericidal and bacteriostatic properties, however, it produces inflammatory effects on the human body. The availability of rapid systems to detect its accidental presence is therefore useful to speed up the control and apply corrective actions. In the present work, a drop casting and easily prepared plastic graphite / PVC electrode decorated with NiO nanostructures has been investigated as

electrochemical sensor for the non-enzymatic amperometric determination of H_2O_2. The catalytic activity, dispersion, and stability of NiO nanostructures mixed with plastic nanocomposite electrode have been studied in detail. The preparation method, particularly the precipitating agents used in the synthesis of NiO nanostructures strongly influenced their morphology and porosity. Further, the electrochemical response of NiO-PE electrodes towards H_2O_2 resulted to be morphology-dependent. The non-enzymatic electrochemical sensor was optimized for the rapid and sensitive detection of H_2O_2 present in milk with no sample pre-treatments. NiO nanoflowers showed the best catalytic activity towards H_2O_2, a linear range that extends up to 4 mM and a LOD of 5 µM (3sd of the blank signal) were obtained.

Introduction

Traditionally, hydrogen peroxide is used in the dairy industry (van Asselt et al., 2017) to increase the shelf-life of unstable foods (Martin et al., 2014), particularly in places in which cooling is not widely available. Hydrogen peroxide can be intentionally added to milk products to stimulate the endogenous lactoperoxidase antibacterial system obtaining either a bacteriostatic or a bactericidal effect (FAO/WHO, 1991; Arefin et al., 2017). It has been shown that hydrogen peroxide, in addition to ozone, alcohol 60%, hypochlorite, peracetic acid, are also effective. Moreover, among others, H_2O_2 offers the advantage of avoiding halogenated substances for disinfection purposes. The Codex Alimentarius (FAO/WHO, 2011), a collection of internationally recognized standards, describes its use to prevent bacterial spoilage of raw milk and despite that it has been shown that hydrogen peroxide added in the range from 0.1% to 0.5% does not damage the nutritional and organoleptic profile of milk (FAO/WHO, 1974), in most of the developed countries the practice of its addition with preservative intention is forbidden. However, the H_2O_2 in milk can arise from cleaning and sanitization treatments at processing plants (Simões et al., 2010).

Hydrogen peroxide it is a chemical with potentially adverse health effects; peroxides in the range of concentration of mM, have been reported to damage the gastro-intestinal cells which can lead to gastritis and inflammation of the intestine (Hemanth et al., 2014; Handford et al., 2016). The need for control for safety purposes induces the optimisation of analytical devices and sensor platforms for the on-site measurements also of hydrogen peroxide. It is generally detected by classical approaches as titration analysis, batch injection analysis (BIA) coupled to amperometric detectors (Silva et al. 2012), or by colorimetric assays (Costa et al. 2020). To reduce the time and costs of the analysis, enzymatic biosensors and non-enzymatic sensors were

optimised (Giannoudi et al. 2006; Shamkhalichenar et al. 2020, Hou et al., 2019). Particularly, the non-enzymatic sensors were developed mainly to overcome the thermal and chemical instability suffered by enzymes. In this frame, nickel oxide (NiO) nanostructures recently emerged as novel monometallic oxide materials with enzyme-like activity, showing several advantages such as low cost, earth-abundance, environmental friendliness, great chemical and thermal stability, and the exceptional catalytic activity principally toward hydrogen peroxide oxidation (Yang et al., 2016; Pan et al., 2015). This great electrocatalytic reactivity was studied with electrodes containing low dimensional NiO nanoflakes arrays (Wang et al., 2012), nanofibers (Wang et al., 2010), nanosheets (Liu et al., 2015) or nanoporous/mesoporous nickel networks (Hou et al., 2019; Veeramani et al., 2015), among others. In the year 2015, Yu et al. showed superior electrocatalytic activity towards H_2O_2 using a NiO/graphene nanocomposite obtained by mixing NiO nanosheets and reduced graphene (Yu et al., 2015). The nanocomposite exhibited high electrocatalytic activity in alkaline media with LOD of 0.766 µM and linear range of 0.25-4.75 mM. Li et al. (2018) synthesized a 3D hierarchical NiO mesoporous nanospheres with enhanced electrochemical performance for the determination of H_2O_2 with a LOD of 0.62 µM, good sensitivity and reliability (Li et al., 2018). Another approach is stabilizing or embeds at the conventional electrode surface, NiO nanostructures by “dip and dry” strategy or by entrapment in ionic polymers (Singh et al., 2020, Hosseinian et al., 2019). However, among all studies highlighted here, there is no evaluation of the catalytic effect of various types of nanostructures performed with a single electrodic platform. The relationship between the nanostructure size and morphology on the non-enzymatic catalysis of H_2O_2, especially in real samples in which matrix effect have to take into account, is an important parameter to consider for future studies.

This paper has investigated the feasibility of bulk modify plastic electrodes (PE) to decorate them with NiO nanostructures of different morphologies. PE is a flexible, lightweight, low-cost and easy to prepare free-standing graphite/PVC-based conductive material obtained by the procedure of plastisol casting at room temperature (Marsilia et al., 2018, Figueredo et al. 2021). The rationale of our approach is to study the possibility to improve the electrochemical properties of pristine PE by taking advantage of the catalytic activity of NiO nanostructures. The aim is optimising an electrochemical sensor to determine non-enzymatically H_2O_2 and we used different NiO nanostructures (Carbone et al. 2021) such as nano/micro flowers and nanoporous structures to investigate their catalytic efficiency, dispersion and stability once mixed in the hybrid-plastic nanocomposite. Finally, milk samples, spiked with hydrogen peroxide were analysed with this NiO-plastic electrode to optimise an easy measurement procedure.

2. Material and methods

2.1 Reagents

All reagents, synthetic graphite (SG), high molecular weight polyvinylchloride powder (PVC), bis(2-ethylhexyl)adipate (BEA) plasticizer, NaOH, triethylamine, urea, $Ni(NO_3)_2$, HNO_3, were purchased from Sigma (Milan, IT). Tetrahydrofuran (THF) was obtained from Alfaesar (VWR-IT).

2.2.1 Equipment

Scanning Electron micrographs (SEMs) were collected at 7 kV and 105 s at 2.5 mA (Zeiss Auriga Field Emission-Scanning Electron Microscope). Textural characteristics were measured according to the B.E.T. method by nitrogen adsorption at 77 K (Tristar 3000, Micromeritics). X-ray diffraction (XRD) spectra were recorded on a Philips X'Pert diffractometer (equipped with a real time multiple strip detector) operated at 40 kV and 40 mA using Ni-filtered Cu-K radiation. Spectra were collected using a step size of 0.02° and a counting time of 10 s per angular abscissa in the range 5–80°. The Philips X'Pert HighScore software was used for phase identification. The mean crystalline size was estimated from the full width at the half maximum (FWHM) of the X-ray diffraction peak using the Scherrer equation (eq.1 in S.I). Voltammetric experiments were performed with a potentiostat/galvanostat CHI 660E (CH Instruments, Inc., Austin, TX-USA). The potentiostat was interfaced with a PC under CHI 19.03 software version control.

2.3 Procedure

2.3.1 Synthesis of NiO nanostructures

NiO nanostructures were prepared by hydrothermal synthesis of $Ni(OH)_2$ using different precipitating agents; NaOH, triethylamine and urea, followed by calcination. NiO morphologies were controlled primarily by tuning the precipitating agent. In a typical synthesis, 50 ml of a solution of $Ni(NO_3)_2$ 0.7 M, was placed in a beaker and kept under stirring at room temperature (RT), till a homogeneous solution was obtained. Afterwards, 50

ml of a solution 1.4 M of precipitating agent was added dropwise. The pH of the solution was adjusted to 8 if necessary, by adding solutions of HNO_3 or NaOH. The slurry was kept stirred for 1h in a water/ice bath, transferred into a 200 mL Teflon-lined stainless steel autoclave (tightly sealed) and heated up to 185°C for 18h in a furnace. After gentle cooling, the slurry was filtered and the powder repeatedly rinsed with distilled water prior to drying it overnight at 80°C. Quotas of the powder precursor were placed in a tubular oven and heated up at a rate of 10° min^{-1} till the target temperature was reached. The calcinations were carried out at 600°C for 2h in air. The corresponding obtained samples synthesized with triethylamine, NaOH and urea were labelled as NiO(A6), NiO(S6) and NiO(U6), respectively. In addition, a portion of the precursor obtained with triethylamine was calcinated 2h at 400°C and the corresponding sample was labelled as NiO(A4).

2.3.2 Plastic electrodes preparation

The electrode was prepared following the procedure previously reported (Marsilia et al 2018) including modifications to add the NiO nanostructures. Briefly, 15 ml of THF was gently poured on 350 mg of SG, 40 mg of PVC and 125 µL of BEA under stirring at room temperature for 40 min. Immediately after sonication for 10 min in a 45 Hz water bath sonicator (Bransonic, Branson Ultrasuoni, Srl, IT), the plastisol was transferred into a glass tray under the fume-hood (20°C and RH% 20 – 25) and left overnight for solvent evaporation to obtain the standard graphite based-electrode (G-PE). To obtain NiO-decorated PE (NiO-PE), NiO nanostructures were added (Table 1) to the plastisol, immediately after sonication, and stirred 10 min before the casting step. Moreover, just for NiO(A6), different amounts (8, 16 or 30 mg) of nanostructured powders were added. As a result, we obtained an electrically conductive film of about 200 µm of thickness from which the electrodes were easily cut to a final geometrical area of 0.25 cm^2 (Figure 1 SI).

Table 1 near here

2.3.3 Electrochemical measurements

A three electrode configuration was adopted using as working electrode the plastic electrode (either G-PE or NiO-PE), $Ag^{+}/AgCl,Cl^{-}_{sat}$ as reference electrode (RE) and Pt-wire as auxiliary electrode (AE). G-PE was used as such, NiO-PE, was pretreated performing 15 sweeps in cyclic voltammetry in the range - 0.4 V and + 1.2 V at a scan rate of 0.05 Vs^{-1} in NaOH 0.1 M. Soon after, amperometry was carried out placing the active NiO-PE electrode in a fresh solution of 0.1 M NaOH, polarized at + 0.2 V and H_2O_2 was added under stirring. A single electrode was used several times, just rinsed with ultrapure water before further use and it was also tested as disposable electrode. The electrodes were disposed in dry waste, following the local rules for waste removal.

2.3.4 Measurements in milk

Milk was purchased from a local market, its pH was raised to 10 with NaOH 1 M and a calibration curve was obtained adding increasing amounts of H_2O_2. The recovery values were calculated with the following equation:

$$\text{Recovery value (\%)} = [(\text{Current value}_{\text{spiked sample}} - \text{Current value}_{\text{raw sample}})/\text{Current value}_{\text{spiked sample}}] \times 100 \quad \text{eq. 1}$$

The "current value $_{\text{raw sample}}$" was the current value measured in milk before it was spiked, and the "Current value $_{\text{spiked sample}}$" was the current value measured with the spiked sample. The recovery test was performed by transferring a volume of 1 ml of fresh milk at pH 10 in the electrochemical cell and by adding H_2O_2 in concentration of 100 µM and 1 mM. All measurements were carried out by amperometry (E vs time), details are available in section 2.3.3.

3. Results and discussion

3.1. NiO-PE electrochemical pattern and relation with morphology of NiO nanostructures

The electroactivity of NiO-PE is related to the redox system Ni/NiO/NiOOH (Lyons et al., 2012). In this equilibrium, NiOOH is the specie involved in the catalytic oxidation of hydrogen peroxide useful for analytical purposes. Accordingly with literature data (Lyons et al, 2012; Liu et al., 2005), NiOOH is electrochemically

generated in the alkaline buffer during the sweeps in CV (eq. 2), then it chemically reacts with H_2O_2 (eq. 3) (Yu et al., 2015; Chang et al., 2008):

$$Ni/NiO + 2OH^- \rightarrow Ni(OH)_2 + OH^- \rightarrow NiOOH + H_2O + e^- \quad \text{eq. 2}$$

$$2\,NiOOH + H_2O_2 \leftrightarrow 2Ni(OH)_2 + O_{2(g)} \quad \text{eq. 3}$$

The electrochemical response of G-PE and NiO-PEs was investigated by cyclic voltammetry (CV) experiments in NaOH 0.1 M. No faradic current was recorded for G-PE (SI Figure X), in the voltage range from - 0.4 V to + 1.3 V. Figure 1 compares all NiOs CVs, details are reported in Table 2 (see also SI). The electrodes prepared from each of the nanostructured NiOs studied displayed the Ni^{2+}/Ni^{3+} redox process at different potentials ($E_p$anodic, i and $E_p$cathodic, i'). Moreover, the oxidation of oxygen (j), not detectable for G-PE (Figure 1, a), was evident at about + 0.75 V for NiO-PE(A4) (Figure 1, a) (Lyons et al., 2012). The NiO-PE(A4) electrode displayed higher current densities among all NiO-PE electrodes and the lowest difference between Ni^{2+}/Ni^{3+} peaks (Figure 1, a i and a i') or in others words, the best reversible behaviour (ΔE = 147 mV). The ΔE value obtained for NiO-PE(A6), other "A" preparation tested (Table 2 and Figure 1, b), was not measurable (Epc was not well defined), and its current density was three times lower in comparison to NiO-PE(A4). To improve NiO-PE(A6) performances, different amounts of NiO(A6) nanostructures (8, 16 and 30 mg) were compared, and the current densities lowered with the increasing amount of NiO nanopowder.

For other preparations, the redox-reversible behavior of Ni^{2+}/Ni^{3+} couple (ΔE value) became sluggish for NiO-PE(U6) > NiO-PE(S6), together with the current density that was 8 times lower with NiO-PE(S6) and about 16 times with NiO-PE(U6) (compared to NiO-PE(A4)), respectively (Figure 1, c, d and Table 2).

Figure 1 near here

Table 2 near here

When consecutive cyclic voltammetric sweeps were carried out, the redox processes of NiO species were better defined (Figure 1, b – e). The voltage was swept 10, 20, 30 and 50 times to tune the pre-anodization step to obtain the reactive NiOOH and enhance the catalytic efficiency at the electrode surface. The current (ipa) values measured at the last cycle of each pre-anodization experiment (Table 2) and their ratio of the current densities (Figure 1, f), are shown. The current increases with sweeps for all NiO-PEs but the efficiency of conversion of NiO into its reactive form level off in comparison to A4.

To assess the active NiO species formed during CVs, equation 3 is applied:

$$\Gamma = Q / nFA \qquad \text{eq. 3(§)}$$

where Γ (mol cm^{-2}) is the surface active specie, Q is the charge obtained by cyclic voltammetry, A is the geometrical electrode surface in cm^2, *n* are the electrons exchanged in redox process, F is the Faraday constant.

The amount of NiOOH formed in NiO-PE (at the 20^{th} sweep) follows the order NiO-PE (A4) > (S6) > (A6) > (U6) (Table 2).

To put shade of light in these results, XRD (Jenkins and Snyder et al., 1996; Pecharsky et al., 2003) patterns of NiO-PEs (Figure 2) were collected and compared with those of G-PE. G-PE shows the typical peaks of the synthetic graphite at 26.6° and 54.7°. On the other hand, NiO-PEs show peaks at 2θ = 37.2°, 43.2° and 62.8°, attributed to (111), (200), (220) reflections of NiO planes, respectively. The peak positions are in agreement with the diffraction data of the standard spectrum for the NiO cubic crystal system (JCPDS card no 47-1049). NiO crystallite size, esteemed by Debye–Scherrer equation (Snyder and Jenkins, 2012; Equation 1 in S.I.), ranged from 20 – 30 nm in all samples prepared. The sharpness and intensity of the peaks indicate the well crystalline nature of NiO (Pecharsky and Zavalij, 2008), meanwhile XRD patterns confirmed that these three morphologies retained the original phase structures (despite of the calcination treatment), even if slightly shift in θ angle were observed among all NiO decorated electrodes.

Figure 2 near here

SEM micrographies of both sides of NiO electrodes were taken at different magnitudes. NiO nanostructures decorating the NiO-PEs can be appreciated, at larger magnifications, in Figure 3. The precipitating agents used in the synthesis of NiO nanostructures determine their morphology and porosity by influencing the bottom-up NiO-PEs structuring. NiO(A4) nanopowder has a flower-like micrometric organization, creates a homogeneous blend at the nanometric level (front side, Figure 3, a) with the nanostructures embedded in the plastic electrode. The plastisol (BEA) somehow fill the internal pores of the NiO micro-flowers maintaining the original organization, as ascertained in the backside of the NiO-PE(A4) electrode (Figure 3.b), where micro-

flowers or portions of them persist (high magnification detail in green circles). Some jagged contour of grains are evident in the red square (Figure 3, b). Grains inhomogeneity is considered as an effect of NiO nanostructures interacting with the components of the BEA and the polar groups of PVC, as can be seen in detail in Figure 5 SI. Exfoliated structures and interlayers, marked with a green square in Figure 3 (b), were produced.

The surface of NiO-PE(S6) and NiO-PE(U6) contains NiO nanostructures always with this shape of flowers but with subtler structures showing different porosity (Figure 3, e – h). NiO-PE(S6) display porous like nanostructures with large holes in the structure, and NiO-PE(U6) contains nanostructures displaying a denser and compact structure. NiO nanostructures were absent on the backside of the NiO-PE(U6), though retaining the alternation between flat and rippled areas. The NiO-PE(S6) obtained with (S6) nanostructures had an even distribution on both sides.

Finally, the synthesis of the NiO(A6) also yields flower-like microstructures, though, on average of larger size in comparison to NiO(A4) (both the nano and the micro-level). The electrodes prepared with increasing amount of NiO(A6) nanostructures were also analyzed by SEM. In Figure 3. (c, d) is possible to appreciate a magnified SEM picture showing the NiO(A6) nanoflowers fragments in the front side of the electrode. Electrodes prepared with different amount of NiO(A6) were compared as can be seen in SI (Figure 3). The NiO-PE prepared with 8 mg of NiO(A4) displays the nanostructures on both sides, the one at intermediate load (16 mg) shows larger portions of the flowers (green circle in SI Figure 3), whereas at the largest load (30 mg), full flowered microstructures are present. It is interesting to note that the amount of NiO(A6) increased respect to the plasticizer (S.I. Table 1 and SI Figure 4a) and when the ratio between these two components was roughly equal to 1 (i.e. A6 30mg), the pristine structure of NiO(A6) nanostructure was better preserved. This seems to confirm that the interactions established between PVC and BEA (plastisol) during electrode formation are likely to involve the NiO nanostructures dispersed in the plastisol (Wypych, 2004; Fu et al., 2008), which seems to preserve the flowers nanostructures shape. A first point of coherence of the results obtained from the SEM and XRD analysis (Figure 1, b) arises after we confirmed the inclusion of the nanoparticles in the PE. The evidence was obtained from the intensity of peaks at $2\theta = 37.2°$, 43.2° and 62.8°, belonging to NiO reflections plane, which concomitantly increased. Moreover, even if some exfoliating effect on NiO nanoparticles was revealed, NiO crystal stability was corroborated as no new phases were detectable.

Based on this evidence, higher current densities measured with NiO-PE(A4) together with the electrochemical pattern during the pre-anodization step (Figure 1, a) is related to some in-homogeneities in the back-side of the electrode with evidence of interlayers displaying better exposure of crystal faces. NiO-A4 heterocomposite

seems to be rich in the number of corners, edges and defects, which enhance their electroactivity. On the other hand, we observed that as the concentration of NiO(A6) (8, 16 and 30 mg) increased, the lower current densities were measured. The fragmentation of the nanoflower-shape was particularly evident for NiO-PE(A6) with 8 mg, but less clear for the other concentrations tested (16 and 30 mg). In this sense, higher NiO(A6) loads seems to introduce defects that foster the interconnection among particles increasing the composite resistivity and reducing the peak current intensity.

Figure 3 near here

3.2 NiO-PE in hydrogen peroxide electrochemical detection

On the basis of the results obtained in this study, NiO-PEs prepared with 8 mg of nanostructures were electrochemically activated performing 20 sweeps in NaOH 0.1 M, then immediately transferred in fresh NaOH 0.1 M to carry out CVs and test the hydrogen peroxide catalysed oxidation (Figure 4).

Hydrogen peroxide 1 mM detected with NiO-PE(A4) produced a four-fold increment in the peak current at 0.4 V with the onset of the oxidation process evident at E = - 0.1 V, substantiating that the electrical wiring in PE is not hindered by the plastic filler (Figure 4, a **iv**). The second addition of H_2O_2 (i.e. 2 mM) (Figure 4, a **v**) produced a proportional current increment.

For seek of comparison, NiO-PE(A6) (Figure 4, b ii and b iii) and NiO-PE(S6) (Figure 4, c ii and c iii) (as NiO-PE(U6), not shown) were tested. The onset of the non-enzymatic oxidation of H_2O_2 was confirmed for NiO-PE(A6) but in NiO-PE(S6) shifted to a slightly more positive potential. For both electrodes, the current densities were lower than those measured with NiO-PE(A4) and a trend with hydrogen peroxide concentration was observed in (S6) but not in (A6) electrode. The results are showing a coherent trend with the amount of NiO-reactive species formed during the step of electrochemical activation i.e. NiO-PE(A6) < NiO-PE(S6) < NiO-PE(A4), previously esteemed (Table 2).

In Figure 4 (a ii) is also evident that no faradic current was observed at G-PE electrode with H_2O_2, apart from a slight increase in the background current vs the fresh buffer (i).

This evidence confirms the formulation stability during the electrocatalytic process of oxidation due, exclusively, to the NiOOH reactive specie. As already stated, the morphology of NiO nanostructures plays a

role in the organization of the structure of the conductive plastic electrode and the catalytic properties are also morphology-dependent.

Figure 4 near here

The amperometric response of H_2O_2 at the NiO-PE(A4) electrode activated and polarized at + 200 mV was measured in 0.1 M NaOH under stirring (Figure 5, a). Each addition of H_2O_2 produced a sharp increment in the current value and the steady-state signal was gained for 3 seconds. Finally, the interference of classical electroactive chemicals, i.e. ascorbic acid (1 mM) and uric acid (1 mM) were tested with a negligible effect on the H_2O_2 oxidation signal. In Figure 5 (b), the calibration plot show a dynamic range from 10 µM to 5 mM with the linear behavior up to 4 mM, a linear fit of $y = 2.8\ 10^{-5}\ b + 2\ 10^{-6}$ ($A\ mM^{-1}$) ($R^2 = 0.990$, $r_{Pearson} = 0.9772$), a LOD (lower limit of detection) of 5 µM (3 times the standard deviation (σ_{blank}) of the background current). Moreover, apart from the recently published impressive results obtained by Balu et al. 2019, that optimized a sensor based on CuO with a LOD of 5.8 nM (Balu et al., 2019), the analytical performances were comparable to those offered by other non-enzymatic sensors (Table 3). In this study we show the advantages of a plastic-like electrically-conductive material obtained with a simple and low cost procedure and used to measure hydrogen peroxide with high reproducibility and sensitivity.

Figure 5 near here

Table 3 near here

Finally, the CVs were carried out in milk with both G-PE and NiO-PE. No signals were observed (Figure 6, i and ii) but the catalysis of H_2O_2 oxidation after hydrogen peroxide addition (Figure 6, iii and iv) was preserved, even if the real sample slightly shifted this oxidation process (vs fresh buffer) to more positive potentials, suggesting that some components, either lipids or proteins (commonly found in milk), fouled the electrode surface.

Figure 6 near here

Recovery tests were performed with NiO-PE(A4) submerged in 1 mL of alkalinized milk containing hydrogen peroxide 0.1 and 1 mM. The recovery values obtained were 111% and 95%, respectively; confirming that the observed fouling effect did not impair the performance of the electrode. These evidences are substantiating that size and morphology of NiO nanostructures strongly influence the electrochemical properties of the electrode (Carbone et al., 2017a; Carbone et al., 2017b; Hall et al., 2014; Wang et al., 2012; Zhang et al., 2010; Lang et al., 2008; Klimov, 2007) and the interest of the researchers aiming to synthetize a wide range of nanoparticles and nanostructures (2D, 3D and hollow) of different morphologies to enhance the electrochemical properties of them (Gund et al., 2014; Offiah et al., 2014; Kim et al., 2013; Liu et al., 2005; Ma and Sun, 2002; Xiang et al., 2002; Liu and Anderson, 1996). Moreover, results show that the NiO electrochemical behavior is not directly related to surface area, but rather depends on the connectivity of crystals and their active sites (Yang et al., 2016; Patra et al., 2015; Zhao et al., 2009).

5. Conclusion

The here obtained electrodes decorated with nano-gardens of NiOs were stable during preparation and during the measurements performed both in fresh buffer and in milk sample. It is worth to note that these electrodes are cost effective and easy to prepare and the performances offered were comparable with those from other electrodes reported in literature. A robust recovery of H_2O_2 in spiked samples is obtained and the need of sample preparation was limited to the rise of the pH gained by adding NaOH solution with negligible interferences from added electroactive interferents. Future investigation will be focus on the determination of H_2O_2 from a wide variety of milk samples. In order to avoid potential interferences effects, dilution or flocculation of proteins and lipids will be considered to validate the proposed sensor for further use.

References

Arefin, S., Sarker, A. H., Islam, A., Harun-Ur-Rashid, & Islam,N. (2017). Use of Hydrogen Peroxide (H_2O_2) in raw cow's milk preservation. *Journal of Advanced Veterinary and Animal Research*, 4, 371–377. https://doi.org/10.5455/javar.2017.d236

Balu, S., Palanisamy, S., Velusamy, V., & Yang, T. C. (2019). Sonochemical synthesis of gum guar biopolymer stabilized copper oxide on exfoliated graphite: application for enhanced electrochemical detection of H_2O_2 in milk and pharmaceutical samples. *Ultrasonics Sonochemistry*, *56*, 254–263. https://doi.org/10.1016/j.ultsonch.2019.04.023

Carbone, M., Bauer, E. M., Micheli, L., & Missori, M. (2017b). NiO morphology dependent optical and electrochemical properties. *Colloids and Surfaces A: Physicochemical and Engineering Aspects*, *532*, 178–182. https://doi.org/10.1016/j.colsurfa.2017.05.046

Carbone, M., Nesticò, A., Bellucci, N., Micheli, L., & Palleschi, G. (2017a). Enhanced performances of sensors based on screen printed electrodes modified with nanosized NiO particles. *Electrochimica Acta*, *246*, 580–587. https://doi.org/10.1016/j.electacta.2017.06.074

Chang, Y., Qiao, J., Liu, Q., Shangguan, L., Ma, X., Shuang, S., & Dong, C. (2008). Electrochemical behavior of hydrogen peroxide at a glassy carbon electrode modified with nickel hydroxide–decorated multiwalled carbon nanotubes. *Analytical Letters*, *41*(17), 3147–3160. https://doi.org/10.1080/00032710802462982

Costa, R. A., Morais, C. L., Rosa, T. R., Filgueiras, P. R., Mendonca, M. S., Pereira, I. E., & Romao, W. (2020). Quantification of milk adulterants (starch, H_2O_2, and NaClO) using colorimetric assays coupled to smartphone image analysis. *Microchemical Journal*, *156*, 104968. https://doi.org/10.1016/j.microc.2020.104968

Dong, S., Xi, J., Wu, Y., Liu, H., Fu, C., Liu, H., & Xiao, F. (2015). High loading MnO_2 nanowires on graphene paper: facile electrochemical synthesis and use as flexible electrode for tracking hydrogen peroxide secretion in live cells. *Analytica Chimica Acta*, *853*, 200–206. https://doi.org/10.1016/j.aca.2014.08.004

FAO/WHO 1991, Codex Alimentarius Commission, Guidelines for the preservation of raw milk by use of the lactoperoxidase system (Cac /gl 13-1991).

FAO/WHO 2011. Milk facts. Rome: Food and Agriculture Organization of the United Nations. Available from: http://www.fao.org/3/i2085e/i2085e00.pdf. Accessed April 20, 2021.

Feng, X., Zhang, Y., Song, J., Chen, N., Zhou, J., Huang, Z., ... & Wang, L. (2015). MnO_2/graphene nanocomposites for nonenzymatic electrochemical detection of hydrogen peroxide. *Electroanalysis*, *27*(2), 353–359. https://doi.org/10.1002/elan.201400481

359 Figueredo, F., Girolametti, F., Aneggi, E., Lekka, M., Annibaldi, A., & Susmel, S. (2021). Plastic electrode
360 decorated with polyhedral anion tetrabutylammonium octamolybdate $[N(C_4H_9)_4]_4$ Mo_8O_{26} for nM phosphate
361 electrochemical detection. *Analytica Chimica Acta*, *1161*, 338469. https://doi.org/10.1016/j.aca.2021.338469

362 Fu, S. Y., Feng, X. Q., Lauke, B., & Mai, Y. W. (2008). Effects of particle size, particle/matrix interface adhesion
363 and particle loading on mechanical properties of particulate–polymer composites. *Composites Part B:*
364 *Engineering*, *39*(6), 933–961. https://doi.org/10.1016/j.compositesb.2008.01.002

365 Giannoudi, L., Piletska, E. V., & Piletsky, S. A. (2006). Development of biosensors for the detection of hydrogen
366 peroxide. In *Biotechnological Applications of Photosynthetic Proteins: Biochips, Biosensors and Biodevices*
367 (pp. 175–191). Springer, Boston, MA.

368 Gund, G. S., Dubal, D. P., Shinde, S. S., & Lokhande, C. D. (2014). Architectured morphologies of chemically
369 prepared NiO/MWCNTs nanohybrid thin films for high performance supercapacitors. *ACS Applied Materials &*
370 *Interfaces*, *6*(5), 3176–3188. https://doi.org/10.1021/am404422g

371 Hall, D. S., Lockwood, D. J., Bock, C., & MacDougall, B. R. (2015). Nickel hydroxides and related materials: a
372 review of their structures, synthesis and properties. *Proceedings of the Royal Society A: Mathematical,*
373 *Physical and Engineering Sciences*, *471*(2174), 20140792. https://doi.org/10.1098/rspa.2014.0792

374 Handford, C. E., Campbell, K., & Elliott, C. T. (2016). Impacts of milk fraud on food safety and nutrition with
375 special emphasis on developing countries. *Comprehensive Reviews in Food Science and Food Safety*, *15*(1),
376 130–142. https://doi.org/10.1111/1541-4337.12181

377 Hemanth, S., & Sukumaran, M. K. (2015). Milk adulteration in Hyderabad, India-a comparative study on the
378 levels of different adulterants present in milk. *Indian Journal of Dairy Science*, *68*(2), 190–192.

379 Hosseinian, M., Darzi, G. N., & Rahimpour, A. (2019). A novel bioelectrochemical sensor based on immobilized
380 urease on the surface of nickel oxide nanoparticle and polypyrrole composite modified Pt electrode.
381 *Electroanalysis*, *31*(12), 2530–2537. https://doi.org/10.1002/elan.201800862

382 Hou, L., Bi, S., Lan, B., Zhao, H., Zhu, L., Xu, Y., & Lu, Y. (2019). A novel and ultrasensitive nonenzymatic
383 glucose sensor based on pulsed laser scribed carbon paper decorated with nanoporous nickel network.
384 *Analytica Chimica Acta*, 1082, 165–175. https://doi.org/10.1016/j.aca.2019.07.056

385 Joint FAO/WHO Expert Committee on Food Additives, & World Health Organization. (1974). *Toxicological*
386 *evaluation of certain food additives with a review of general principles and of specifications: seventeenth report*

of the Joint FAO/WHO Expert Committee on Food Additives, Geneva, 25 June-4 July 1973. World Health Organization.

Kim, S. I., Lee, J. S., Ahn, H. J., Song, H. K., & Jang, J. H. (2013). Facile route to an efficient NiO supercapacitor with a three-dimensional nanonetwork morphology. *ACS Applied Materials & Interfaces*, *5*(5), 1596–1603. https://doi.org/10.1021/am3021894

Klimov, V. I. (2007). Spectral and dynamical properties of multiexcitons in semiconductor nanocrystals. *Annual Reviews of Physical Chemistry*, *58*, 635–673. https://doi.org/10.1146/annurev.physchem.58.032806.104537

Lang, J. W., Kong, L. B., Wu, W. J., Luo, Y. C., & Kang, L. (2008). Facile approach to prepare loose-packed NiO nano-flakes materials for supercapacitors. *Chemical Communications*, 35, 4213–4215. https://doi.org/10.1016/10.1039/B800264A

Li, Q., Gao, W., Zhang, X., Liu, H., Dou, M., Zhang, Z., & Wang, F. (2018). Mesoporous NiO nanosphere: A sensitive strain sensor for determination of hydrogen peroxide. *RSC Advances*, 8, 13401–13407. https://doi.org/10.1039/c8ra01313f

Liu, K. C., & Anderson, M. A. (1996). Porous nickel oxide/nickel films for electrochemical capacitors. *Journal of the Electrochemical Society*, *143*(1), 124. https://doi.org/10.1149/1.1836396

Liu, W., Zhang, H., Yang, B., Li, Z., Lei, L., & Zhang, X. (2015). A non-enzymatic hydrogen peroxide sensor based on vertical NiO nanosheets supported on the graphite sheet. Journal of Electroanalytical Chemistry, 749, 62–7. https://doi.org/10.1016/j.jelechem.2015.04.037

Liu, Y. Q., & Shen, H. X. (2005). Preparation of nickel hydroxide modified glassy carbon electrode and its electrochemical behavior. *Journal of Analytical Science*, *21*(4), 378.

Lyons, M. E. G., Doyle, R. L., Godwin, I., O'Brien, M., & Russell, L. (2012). Hydrous nickel oxide: redox switching and the oxygen evolution reaction in aqueous alkaline solution. *Journal of the Electrochemical Society*, *159*(12), H932. https://doi.org/10.1149/2.078212jes

Ma, C. L., & Sun, X. D. (2002). Preparation of nanocrystalline metal oxide powders with the surfactant-mediated method. *Inorganic Chemistry Communications*, *5*(10), 751–755. https://doi.org/10.1016/S1387-7003(02)00546-4

Marsilia, M., & Susmel, S. (2018). Free-standing Plastic electrodes: Formulation, electrochemical characterization and application to dopamine detection. *Sensors and Actuators B: Chemical*, *255*, 1087–1096. https://doi.org/10.1016/j.snb.2017.08.052

Martin, N. H., Friedlander, A., Mok, A., Kent, D., Wiedmann, M., & Boor, K. J. (2014). Peroxide test strips detect added hydrogen peroxide in raw milk at levels affecting bacterial load. *Journal of Food Protection*, *77*(10), 1809–1813. https://doi.org/10.4315/0362-028X.JFP-14-074

Offiah, S. U., Nwodo, M. O., Nwanya, A. C., Ezugwu, S. C., Agbo, S. N., Ugwuoke, P. U., ... & Ezema, F. I. (2014). Effects of post-thermal treatments on morphological and optical properties of NiO/Ni (OH) 2 thin films synthesized by solution growth. *Optik*, *125*(12), 2905–2908. https://doi.org/10.1016/j.ijleo.2013.11.073

Pan, Y., Liu, Y., & Liu, C. (2015). Nanostructured nickel phosphide supported on carbon nanospheres: Synthesis and application as an efficient electrocatalyst for hydrogen evolution. *Journal of Power Sources*, 285, 169–177. https://doi.org/10.1016/j.jpowsour.2015.03.097

Patra, A. K., Kundu, S. K., Kim, D., & Bhaumik, A. (2015). Controlled Synthesis of a Hexagonal-Shaped NiO Nanocatalyst with Highly Reactive Facets {1 1 0} and Its Catalytic Activity. *ChemCatChem*, *7*(5), 791–798. https://doi.org/10.1002/cctc.201402871

Pecharsky, V., & Zavalij, P. (2008). Fundamentals of powder diffraction and structural characterization of materials. Springer Science & Business Media.

Shamkhalichenar, H., & Choi, J. W. (2020). Non-enzymatic hydrogen peroxide electrochemical sensors based on reduced graphene oxide. *Journal of the Electrochemical Society*, *167*(3), 037531. https://doi.org/10.1149/1945-7111/ab644a

Silva, R. A., Montes, R. H., Richter, E. M., & Munoz, R. A. (2012). Rapid and selective determination of hydrogen peroxide residues in milk by batch injection analysis with amperometric detection. *Food Chemistry*, 133(1), 200–204. https://doi.org/10.1016/j.foodchem.2012.01.003

Simões, M., Simões, L. C., & Vieira, M. J. (2010). A review of current and emergent biofilm control strategies. *LWT-Food Science and Technology*, *43*(4), 573–583. https://doi.org/10.1016/j.lwt.2009.12.008

Singh, P., & Shukla, S. K. (2020). A structurally aligned nickel oxide encapsulated polypyrrole nanocomposite for hydrogen peroxide sensing. *Dalton Transactions*, 49(25), 8744–8754. https://doi.org/10.1039/d0dt01847c

Snyder, R. L., & Jenkins, R. (2012). *Introduction to X-ray powder diffractometry*. Wiley-Interscience.

van Asselt, E. D., Van der Fels-Klerx, H. J., Marvin, H. J. P., Van Bokhorst-van de Veen, H., & Groot, M. N. (2017). Overview of food safety hazards in the European dairy supply chain. *Comprehensive Reviews in Food Science and Food Safety*, 16(1), 59–75. https://doi.org/10.1111/1541-4337.12245

Veeramani, V., Madhu, R., Chen, S. M., Veerakumar, P., Hung, C. T., & Liu, S. B. (2015). Heteroatom-enriched porous carbon/nickel oxide nanocomposites as enzyme-free highly sensitive sensors for detection of glucose. *Sensors and Actuators B: Chemical*, 221, 1384–1390. https://doi.org/10.1016/j.snb.2015.08.007

Wang, G. P., Zhang, L., & Zhang, J. (2012). A review of electrode materials for electrochemical supercapacitors. *Chemical Society Reviews*. 41, 797–828. https://doi.org/10.1039/c1cs15060j

Wang, K., Huang, J., & Wei, Z. (2010). Conducting polyaniline nanowire arrays for high performance supercapacitors. *The Journal of Physical Chemistry C*, 114, 8062−8067. https://doi.org/10.1021/jp9113255

Wypych, G. (2004). *Handbook of plasticizers*. ChemTec Publishing.

Xiang, L., Deng, X. Y., & Jin, Y. (2002). Experimental study on synthesis of NiO nano-particles. *Scripta Materialia*, *47*(4), 219–224. https://doi.org/10.1016/S1359-6462(02)00108-2

Xu, F., Deng, M., Li, G., Chen, S., & Wang, L. (2013). Electrochemical behavior of cuprous oxide–reduced graphene oxide nanocomposites and their application in nonenzymatic hydrogen peroxide sensing. *Electrochimica Acta*, *88*, 59–65. https://doi.org/10.1016/j.electacta.2012.10.070

Yang, L., Gao, M., Dai, B., Guo, X., Liu, Z., & Peng, B. (2016). An efficient NiS@N/S-C hybrid oxygen evolution electrocatalyst derived from metal-organic framework. *Electrochimica Acta*, 191, 813–820. https://doi.org/10.1016/j.electacta.2016.01.160

Yang, L., Gao, M., Dai, B., Guo, X., Liu, Z., & Peng, B. (2016). An efficient NiS@ N/SC hybrid oxygen evolution electrocatalyst derived from metal-organic framework. *Electrochimica Acta*, *191*, 813–820. https://doi.org/10.1016/j.electacta.2016.01.160

Yu, Z., Li, H., Zhang, X., Liu, N., & Zhang, X. (2015). NiO/graphene nanocomposite for determination of H2O2 with a low detection limit. *Talanta*, 144, 1–5. https://doi.org/10.1016/j.talanta.2015.05.070

Zhang, J., Kong, L. B., Cai, J. J., Li, H., Luo, Y. C., & Kang, L. (2010). Hierarchically porous nickel hydroxide/mesoporous carbon composite materials for electrochemical capacitors. *Microporous and Mesoporous Materials*, *132*(1–2), 154–162. https://doi.org/10.1016/j.micromeso.2010.02.013

Zhang, Y., Bai, X., Wang, X., Shiu, K. K., Zhu, Y., & Jiang, H. (2014). Highly sensitive graphene–Pt nanocomposites amperometric biosensor and its application in living cell H2O2 detection. *Analytical Chemistry*, *86*(19), 9459–9465. https://doi.org/10.1021/ac5009699

Zhang, Y., Yang, W., Wang, Y., Jia, J., & Wang, J. (2013). Nonenzymatic hydrogen peroxide sensor based on a glassy carbon electrode modified with electrospun PdO-NiO composite nanofibers. *Microchimica Acta*, *180*(11–12), 1085–1091. https://doi.org/10.1007/s00604-013-1033-4

Zhao, B., Ke, X. K., Bao, J. H., Wang, C. L., Dong, L., Chen, Y. W., & Chen, H. L. (2009). Synthesis of flower-like NiO and effects of morphology on its catalytic properties. *The Journal of Physical Chemistry C*, *113*(32), 14440–14447. https://doi.org/10.1021/jp904186k

NiO-*nanoflowers* decorating a plastic electrode for the non-enzymatic amperometric detection of H_2O_2 in milk: old issue, new challenge

M. Carbone [a], E. Aneggi [b], F. Figueredo [c,d] and S. Susmel [c],*

Tables

Table 1. Electrodes and condition adopted for synthesis of different NiO nanostructures

Electrode	*NiO nanostructures*	*Precipitating agent*	*Calcination temperature (°C)*	*NiO shape*
G-PE	-	-	-	-
NiO-PE(A6)	NiO **(A6)**	Triethylamine	600	Nanoflower
NiO-PE(A4)	NiO **(A4)**	Triethylamine	400	Nanoflower
NiO-PE(S6)	NiO **(S6)**	NaOH	600	Nanoporous
NiO-PE(U6)	NiO **(U6)**	Urea	600	Nanoporous

Table 2. Efficiency of conversion of NiO into active specie (mol cm^{-2}) generated by different sweeps of cyclic voltammetry.

NiO -PE	***Current (µA)***				***Amount (nmol cm^{-2})***	***Epa (mV)***	***Epc (mV)***	ΔE ***(mV)***	E_{O2} ***(mV)***
	10th sweeps	20th sw.	30th sw.	50th sw.	at 20th sw. (eq.2 §)	at 20th			
A4	120 (RSD 8 %)	270 (RSD4.8%)	400 (RSD7.2%)	520 (RSD 10%)	8.1	+ 490	+ 343	147	+ 650
A6	28 (RSD 9 %)	35 (RSD 10%)	60 (RSD 9 %)	72 (RSD 8.6%)	1.1	+ 600	N.D.	N.D.	+ 610
S6	54 (RSD 5 %)	89 (RSD5.5%)	120 (RSD7.1%)	140 (RSD 10%)	2.7	+ 553	+358	195	+ 690
U6	7.8 (RSD 4 %)	22 (RSD4.5%)	12 (RSD 4.1%)	14 (RSD 5%)	0.7	+ 553	+366	187	+ 700

RSD%: relative standard deviation calculated from 3 activation tests (n = 3) performed using NiO-PE cut from electrode prepared at different times

Table 3: Comparison of performances offered by NiO-PE(A4) and those reported in literature.

Electrode materials	**Linear range (mM)**	**Sensitivity**	**LOD (μM)**	**Ref.**
NiO nanospheres/GCE	0.01-0.8	236.7 μA mM^{-1} cm^{-2}	0.62	Li et al., 2018
NiO/graphene/GCE	0.25-4.75	591 μA mM^{-1} cm^{-2}	0.76	Yu et al., 2015
NiO films/GS	Up to 2.5	409.7 μA mM^{-1} cm^{-2}	4.8	Liu et al., 2015
NiO nanosheets/GS	Up to 4	1077 μA mM^{-1} cm^{-2}	0.4	Liu et al., 2015
MnO_2/ERGO	0.1-45.4	59 μA mM^{-1} cm^{-2}	10	Dong et al., 2015
Graphene/MnO_2/GCE	0.01-0.09 and 0.2-0.9	/	2	Feng et al., 2015
RGO-Pt/GCE	5 10^{-4}-3.47	459 mA M^{-1} cm^{-2}	0.2	Zhang et al., 2014
PdO-NiO nanofibers/GCE	5 10^{-3}-19	583.43 μA mM^{-1} cm^{-2}	2.94	Zhang et al., 2013
RGO/Cu_2O composite/GCE	0.03 - 12.8	19.5 μA μM^{-1}	21.7	Xu et al., 2013
NiO-PE(A4)	Up to 4 mM	25 μA mM^{-1} cm^{-2}	5	This study

CGE: Glassy carbon electrode; RGO: Reduced graphene oxide; GS: graphite sheets; ERGO: electrochemical reduced graphene oxide

NiO-*nanoflowers* decorating a plastic electrode for the non-enzymatic amperometric detection of H_2O_2 in milk: old issue, new challenge

M. Carbone [a], E. Aneggi [b], F. Figueredo [c,d] and S. Susmel [c],*

FIGURES

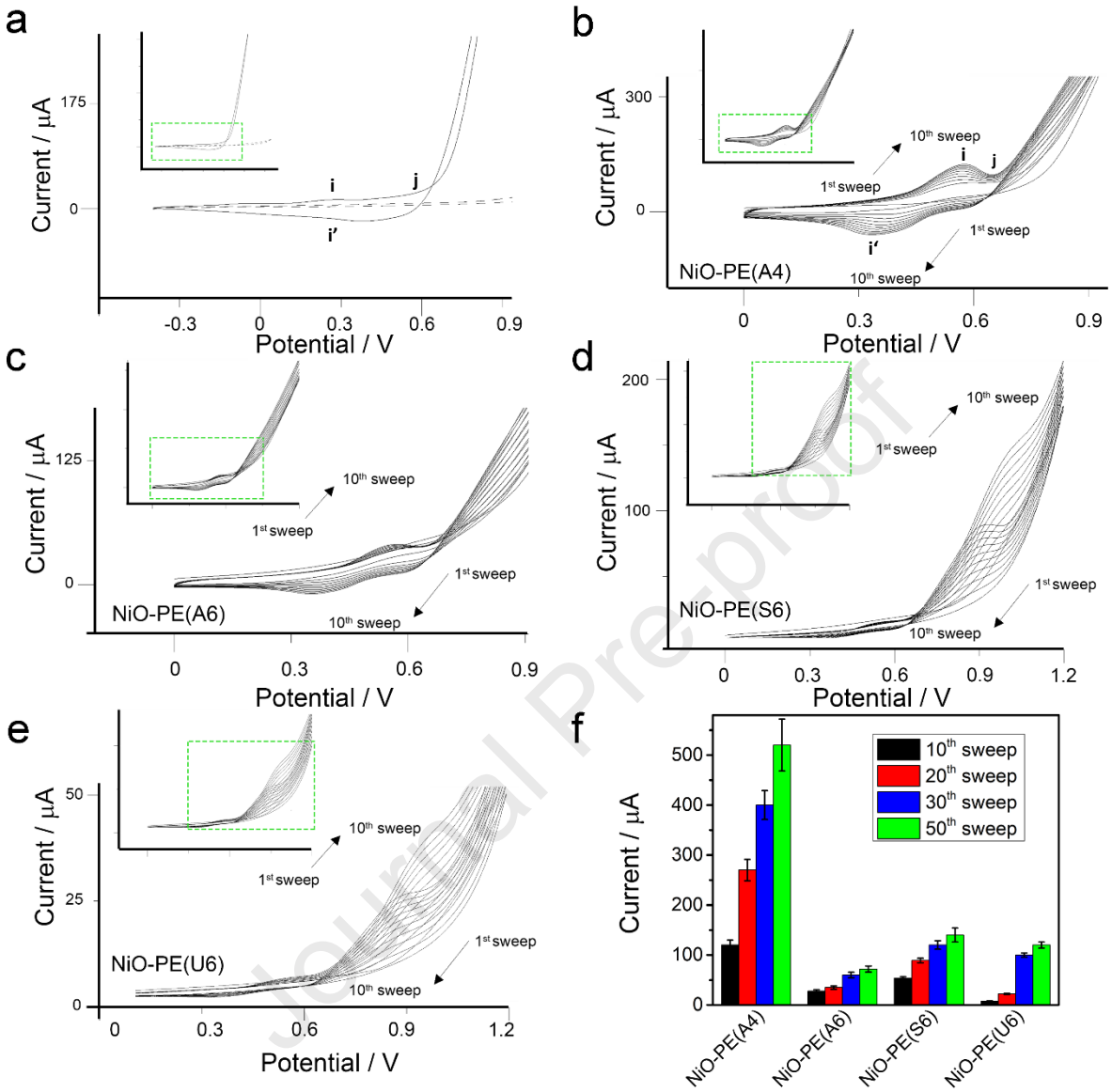

Figure 1. Electrochemical activation of NiO-PE electrodes. (a) Cyclic voltammetry results of G-PE (dash line) and NiO-PE(A4) (continuous line) for the first cycle. (b) NiO-PE(A4) electrode, (c) NiO-PE(A6) electrode, (d) NiO-PE(S6) electrode, (e) NiO-PE(U6) electrode. Inset show the entire cyclic voltammetry range. (f) Current values obtained for the anodic peak at the end of the 10th, 20th, 30th and 50th cycle.

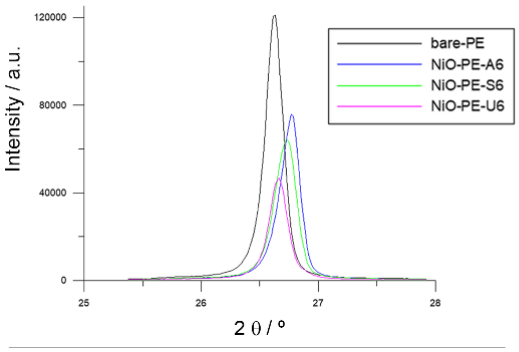

Figure 2: XRD pattern for graphite signal in bare-PE (26.62°), and NiO-PE(U6) (26.66°), NiO-PE(S6) (26.73°) and NiO-PE(A6) (26.77°). The NiO-PE electrodes were prepared with 8 mg of the respective nanopowder.

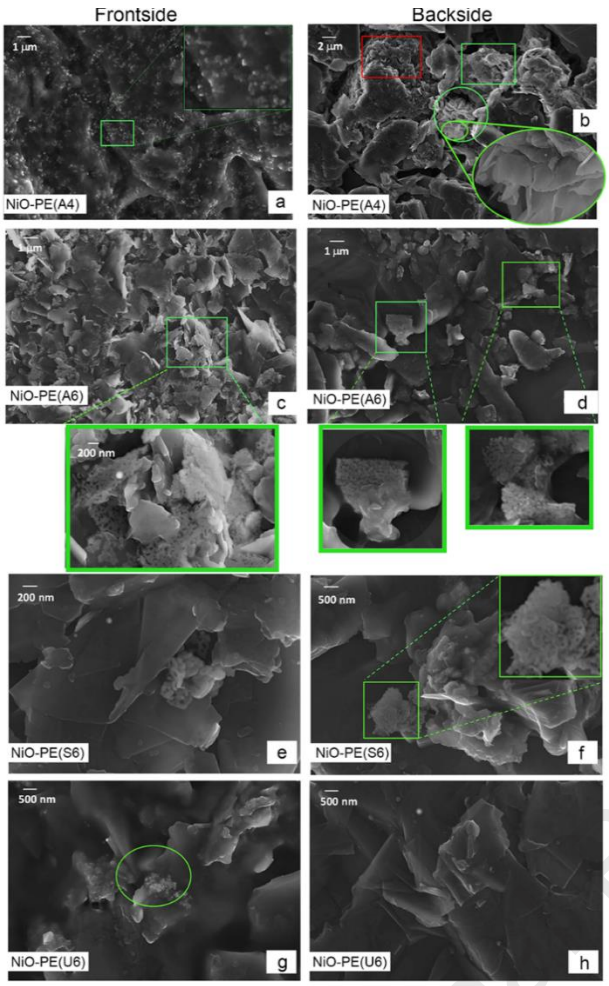

Figure 3. SEM pictures of both front-side and back-side of (a, b) NiO-PE(A4), (c, d) NiO-PE(A6), (e, f) NiO-PE(S6) and (g, h) NiO-PE(U6).

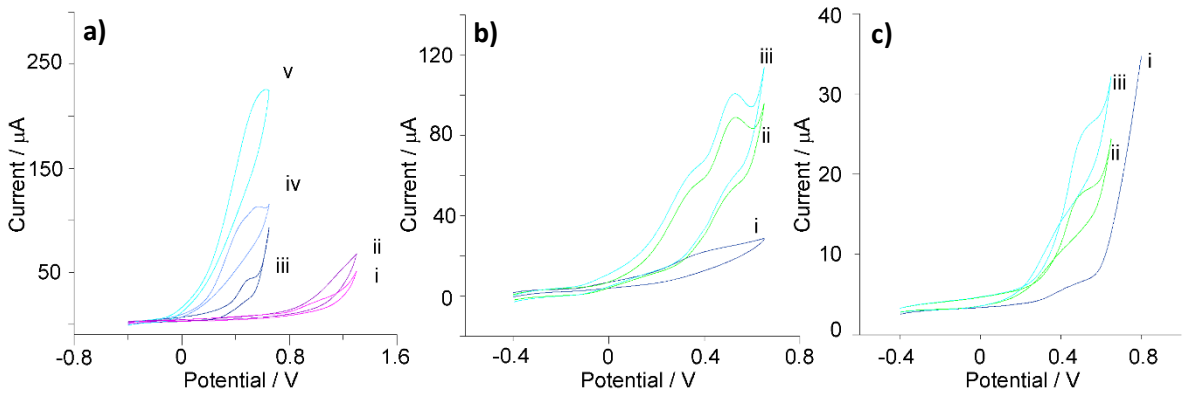

Figure 4. Electrochemical response of NiO-PE electrodes towards H_2O_2. (a) Cyclic voltammetry plots of (i) G-PE in NaOH 0.1 mM and (ii) G-PE in NaOH 0.1 mM with H_2O_2 2 mM, (iii) NiO-PE(A4) in NaOH 0.1 mM and (iv) NiO-PE(A4) in NaOH 0.1 mM with 1 mM of H_2O_2 and (v) with 2 mM of H_2O_2. (b) Cyclic voltammetry plots of NiO-PE(A6) in (i) NaOH 0.1 mM, (ii) NaOH 0.1 mM with 1 mM of H_2O_2 and (iii) with 2 mM of H_2O_2. (c) Cyclic voltammetry plots of NiO-PE(S6) in (i) NaOH 0.1 mM, (ii) NaOH 0.1 mM with 1 mM of H_2O_2 and (iii) with 2 mM of H_2O_2. In all cases the electrodes were produced with 8 mg on NiO nanopowder. Scan rate 50 mV s^{-1}.

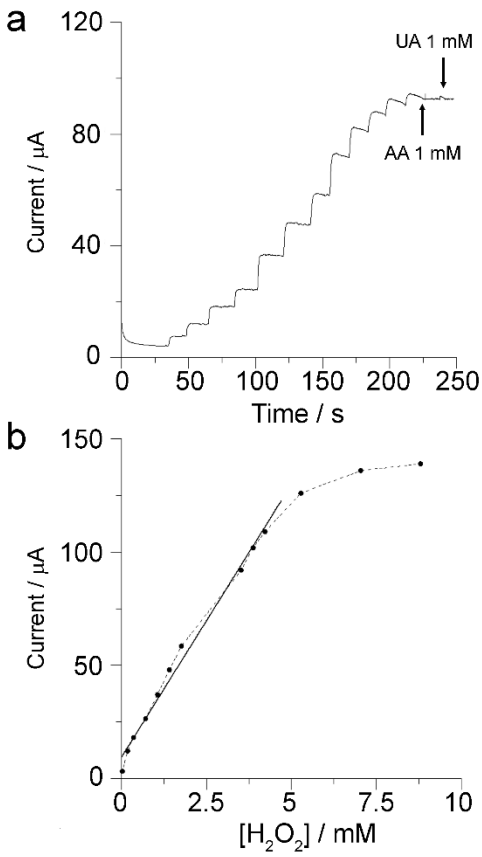

Figure 5. (a) Amperometric response of activated NiO-PE(A4) towards the addition of H_2O_2 applying a polarization potential of + 0.2 V in NaOH 0.1 M. The test of interference was performed with 1 mM of ascorbic acid (AA) and 1 mM of uric acid (UA). (b) Calibration plot obtained after performing three independent experiments (RSD 6%).

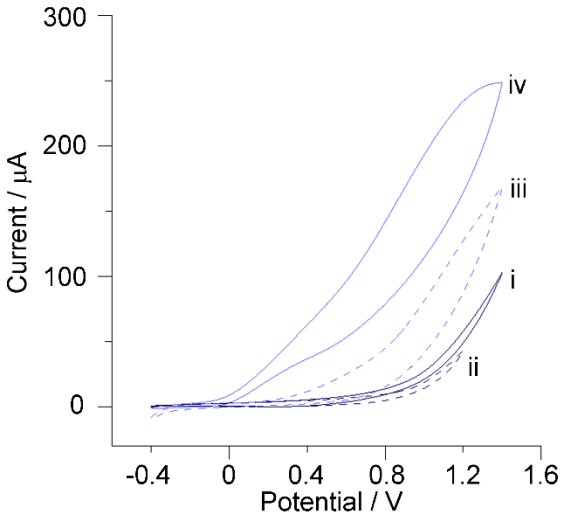

Figure 6. Cyclic voltammetry plots of (i) G-PE in milk at pH 10, (ii) NiO-PE(A4) in milk at pH 10 and spiked with (iii) 1 mM and (iv) 2 mM of H_2O_2. Scan rate 50 mV s^{-1}.

NiO-*nanoflowers* decorating a plastic electrode for the non-enzymatic amperometric detection of H_2O_2 in milk: old issue, new challenge

M. Carbone [a], E. Aneggi [b], F. Figueredo [c,d] and S. Susmel [c],*

Hightlights

- μM detection of residual hydrogen peroxide in milk
- Detection with no sample pre-treatments
- Non-conventional plastic electrode, NiO decorated, for a non-enzymatic amperometric detection
- A cheap and easy way to prepare plastic electrodes containing nanostructures
- The catalytic activity of various NiO nanostructures decorating plastic electrode were studied

Declaration of interests

☒ The authors declare that they have no known competing financial interests or personal relationships that could have appeared to influence the work reported in this paper.

☐The authors declare the following financial interests/personal relationships which may be considered as potential competing interests: